Supporting Information

Leone et al. 10.1073/pnas.1421202112

SI Materials and Methods

Decomposition of the Calculated Free Energy of Selectivity. To evaluate the relative contribution of local and remote factors to the calculated value of $\Delta\Delta G_{sel}$ (Eq. **6**) between the *I. tartaricus* and *E. hirae* rings, both molecular systems were divided into three groups of atoms. For the *I. tartaricus* ring, the first group includes E65 and the bound Na^+/H^+ in one of the ion-binding sites; the second group includes residues Q32, V63, S66, T67, and Y70, plus a bound a structural water molecule, in the same binding site; and the third group comprises all other atoms in the system (protein, water, lipid, ions). For the *E. hirae* ring, the first group includes E139 in one of the ion-binding sites, plus the bound Na^+/H^+; the second group includes L61, T64, Q65, Y68, and Q110 in the same binding site; and the third group includes the rest of the system. If **X**, **Y**, and **Z** denote the coordinates of the atoms in each group, the potential energy function for a given ion-bound state i may be written as follows:

$$U^i(\mathbf{X},\mathbf{Y},\mathbf{Z}) = U^i_{\text{self}}(\mathbf{X}) + U^i_{\text{self}}(\mathbf{Y},\mathbf{Z}) + U^i_{\text{inter}}(\mathbf{X},\mathbf{Y}) + U^i_{\text{inter}}(\mathbf{X},\mathbf{Z}), \quad \textbf{[S1]}$$

where U_{self} refers to self-interactions within a given group of atoms and U_{inter} refers to cross-interactions between two groups. (When long-range electrostatic interactions are calculated using the particle mesh Ewald method, Eq. **S1** is an approximation. For the systems simulated in this study, the difference between the left and right sides of Eq. **S1** is in the order of 10^{-4} kcal/mol.) If $i = 0$ denotes the Na^+-bound state, and $i = 1$ denotes the H^+-bound state, the dual-topology potential-energy function used in our free-energy perturbation (FEP) calculations would read as follows:

$$\begin{aligned} U(\lambda) = {} & \lambda\left[U^1_{\text{self}}(\mathbf{X}^1) + U^1_{\text{self}}(\mathbf{Y},\mathbf{Z}) + U^1_{\text{inter}}(\mathbf{X}^1,\mathbf{Y}) + U^1_{\text{inter}}(\mathbf{X}^1,\mathbf{Z})\right] \\ & + (1-\lambda)\left[U^0_{\text{self}}(\mathbf{X}^0) + U^0_{\text{self}}(\mathbf{Y},\mathbf{Z}) + U^0_{\text{inter}}(\mathbf{X}^0,\mathbf{Y})\right. \\ & \left. + U^0_{\text{inter}}(\mathbf{X}^0,\mathbf{Z})\right], \end{aligned} \quad \textbf{[S2]}$$

where λ denotes the coupling parameter used to control the transformation between the two end states. Note that the dual-topology scheme pertains only to the degrees of freedom represented by **X**, and therefore we differentiate $\mathbf{X}^1$ and $\mathbf{X}^0$. However, the self-energy terms that pertain to **Y** and **Z** are identical. Therefore, Eq. **S2** can be simplified as follows:

$$\begin{aligned} U(\lambda) = {} & \lambda\left[U^1_{\text{self}}(\mathbf{X}^1) + U^1_{\text{inter}}(\mathbf{X}^1,\mathbf{Y}) + U^1_{\text{inter}}(\mathbf{X}^1,\mathbf{Z})\right] \\ & + (1-\lambda)\left[U^0_{\text{self}}(\mathbf{X}^0) + U^0_{\text{inter}}(\mathbf{X}^0,\mathbf{Y}) + U^0_{\text{inter}}(\mathbf{X}^0,\mathbf{Z})\right] \\ & + U_{\text{self}}(\mathbf{Y},\mathbf{Z}). \end{aligned} \quad \textbf{[S3]}$$

In the FEP scheme, the free-energy difference between the Na^+- and H^+-bound states is defined as follows:

$$\Delta G_{\text{FEP}} = -\sum_{j=1}^{n} k_B T \log\left\langle \exp\left\{-\frac{1}{k_B T}\left[U(\lambda_{j+1}) - U(\lambda_j)\right]\right\}\right\rangle_{\lambda_j}, \quad \textbf{[S4]}$$

where the j index refers to n intermediate values of λ between 0 and 1, and the angle brackets denote a time average over a simulation in which the coupling parameter in Eq. **2** equals to λ_j. Provided that the typical differences between λ_{j+1} and λ_j values are sufficiently small, we can assume that $[U(\lambda_{j+1}) - U(\lambda_j)] << k_B T$, and thus Eq. **S4** can be approximated as follows:

$$\begin{aligned} \Delta G_{\text{FEP}} &\approx -\sum_{j=1}^{n} k_B T \log\left\langle 1 - \frac{1}{k_B T}\left[U(\lambda_{j+1}) - U(\lambda_j)\right]\right\rangle_{\lambda_j} \\ &\approx \sum_{j=1}^{n}\left\langle U(\lambda_{j+1}) - U(\lambda_j)\right\rangle_{\lambda_j}. \end{aligned} \quad \textbf{[S5]}$$

Introducing Eq. **S3** into Eq. **S5** leads to the following:

$$\begin{aligned} \Delta G_{\text{FEP}} \approx \sum_{j=1}^{n}(\lambda_{j+1} - \lambda_j)\Big[& \left\langle \Delta U_{\text{self}}(\mathbf{X})\right\rangle_{\lambda_j} + \left\langle \Delta U_{\text{inter}}(\mathbf{X},\mathbf{Y})\right\rangle_{\lambda_j} \\ & + \left\langle \Delta U_{\text{inter}}(\mathbf{X},\mathbf{Z})\right\rangle_{\lambda_j}\Big], \end{aligned} \quad \textbf{[S6]}$$

where ΔU denotes difference in the potential energy terms U^1 and U^0 for the relevant subset of coordinates. Note that a formulation of the free energy as in the thermodynamic integration (TI) method leads to an expression analogous to that in Eq. **S6**:

$$\begin{aligned} \Delta G_{\text{TI}} &= \int_0^1 \left\langle \frac{\partial U(\lambda)}{\partial \lambda}\right\rangle d\lambda = \sum_{j=1}^{n}\left\langle \frac{\partial U(\lambda)}{\partial \lambda}\right\rangle_{\lambda_j}\Delta\lambda \\ &= \sum_{j=1}^{n}\Delta\lambda\left[\left\langle \Delta U_{\text{self}}(\mathbf{X})\right\rangle_{\lambda_j} + \left\langle \Delta U_{\text{inter}}(\mathbf{X},\mathbf{Y})\right\rangle_{\lambda_j} + \left\langle \Delta U_{\text{inter}}(\mathbf{X},\mathbf{Z})\right\rangle_{\lambda_j}\right]. \end{aligned} \quad \textbf{[S7]}$$

Eqs. **S6** and **S7** permit us to assess the extent to which local (i.e., **X** and **Y**) or remote (i.e., **Z**) interactions contribute to the difference in the free energy of selectivity of the two systems considered. Specifically, the breakdown in Fig. 4*B* corresponds to the following:

$$\Delta\Delta G_{\text{TI}}(\text{site}) = \sum_{j=1}^{n}(\lambda_{j+1} - \lambda_j)\left[\left\langle \Delta\Delta U_{\text{self}}(\mathbf{X})\right\rangle_{\lambda_j} + \left\langle \Delta\Delta U_{\text{inter}}(\mathbf{X},\mathbf{Y})\right\rangle_{\lambda_j}\right], \quad \textbf{[S8]}$$

$$\Delta\Delta G_{\text{TI}}(\text{rest}) = \sum_{j=1}^{n}(\lambda_{j+1} - \lambda_j)\left\langle \Delta\Delta U_{\text{inter}}(\mathbf{X},\mathbf{Z})\right\rangle_{\lambda_j}, \quad \textbf{[S9]}$$

$$\Delta\Delta G_{\text{TI}}(\text{total}) = \Delta\Delta G_{\text{TI}}(\text{site}) + \Delta\Delta G_{\text{TI}}(\text{rest}). \quad \textbf{[S10]}$$

Water Occupancy in the H^+-Bound State of the *I. tartaricus* Binding Site. The crystal structure of the Na^+-bound state of the *I. tartaricus* c-ring shows a water molecule co-coordinating the ion. Whether or not this water molecule remains in the H^+ bound state is a priori unknown. However, the binding free energy of this water molecule to the H^+-bound state can be deduced by comparing the calculated free-energies differences between the Na^+- and H^+-bound states in either case. When it is assumed that the water molecule remains in the H^+-bound state, i.e., case a in Fig. 4*A*, the

alchemical transformation between the Na^+- and H^+-bound states pertains only the carboxyl group of E65 and the ion; i.e., the water molecule is coupled to the molecular system throughout the FEP simulation. In this case, the following:

$$\Delta G^{(a)}_{sel}(Na^+ \rightarrow H^+) = \Delta G_{site}(E65 : Na^+ \rightarrow E65 : H^+) - \Delta G_{hyd}(E65 : Na^+ \rightarrow E65 : H^+). \quad \textbf{[S11]}$$

However, if it is assumed that the water molecule is not present in the H^+-bound state, i.e., case b in Fig. 4*A*, it is necessary to decouple it from the molecular system as the Na^+-bound state is transformed in the H^+-bound state. In practice, the water molecule is artificially restrained to remain within the binding site as it is decoupled from the system, so as to facilitate the convergence of the calculation. We achieve this through distance restraints to T67:Oγ and A64:O. The free energy of selectivity in this case is as follows:

$$\Delta G^{(b)}_{sel}(Na^+ \rightarrow H^+) = \Delta G_{site}(E65 : Na^+ : W \rightarrow E65 : H^+) - \Delta G_{hyd}(E65 : Na^+ \rightarrow E65 : H^+) + \Delta G_{hyd}(W) + k_B T \log \frac{V_{site}}{V^o}. \quad \textbf{[S12]}$$

The last two terms in Eq. **S12** reflect the energetic gain associated with the release of the water molecule into the bulk. The first term, $\Delta G_{hyd}(W)$, is the hydration free energy of the water molecule, which is computed separately (−6.5 kcal/mol); the second term reflects the gain in conformational entropy. V^o is the standard-state volume, i.e., the volume accessible at a concentration of 1 M, or 1,661 Å^3. V_{site} is the volume accessible to the water molecule in the decoupled state. This volume is limited, owing to the distance restraints imposed during the calculation; specifically, this value was estimated to be ∼111 Å^3. Note that the precise choice of restraints will affect the value of V_{site}, but also the value of ΔG_{site} resulting from the alchemical transformation; therefore, ΔG_{sel} is not dependent on this choice.

To calculate the standard binding free energy of the water molecule to the H^+-bound state, a similar alchemical transformation could be used:

$$\Delta G^o_b(W) = \Delta G_{site}(E65 : H^+ : W \rightarrow E65 : H^+) - \Delta G_{hyd}(W) + k_B T \log \frac{V_{site}}{V^o}. \quad \textbf{[S13]}$$

Note, however, that this transformation is related to those in Eqs. **S11** and **S12** as follows:

$$\Delta G_{site}(E65 : Na^+ : W \rightarrow E65 : H^+) = \Delta G_{site}(E65 : Na^+ : W \rightarrow E65 : H^+ : W) + \Delta G_{site}(E65 : H^+ : W \rightarrow E65 : H^+). \quad \textbf{[S14]}$$

Therefore, the binding free energy of the water molecule to the H^+ bound state is simply the following:

$$\Delta G^o_b(W) = \Delta G^{(b)}_{sel}(Na^+ \rightarrow H^+) - \Delta G^{(a)}_{sel}(Na^+ \rightarrow H^+). \quad \textbf{[S15]}$$

That is, by comparing the values of ΔG_{sel} in cases a and b, we circumvent a calculation in which only the water molecule in question is decoupled from the H^+-bound state. From the data shown in Fig. 4*A*, the calculated value of $\Delta G_b{}^o$ (W) is −1.6 kcal/mol. That is, binding of the water to the H^+-bound state is energetically favorable. The corresponding dissociation constant,

$$K_d = C^o \exp\left\{\frac{\Delta G^o_b(W)}{k_B T}\right\}, \quad \textbf{[S16]}$$

is therefore 69 mM (where C^o = 1 M). Thus, the probability of occupancy, $P = [1 + K_d/C_w]^{-1} = 0.9987$ (C_w = 55.5 M).

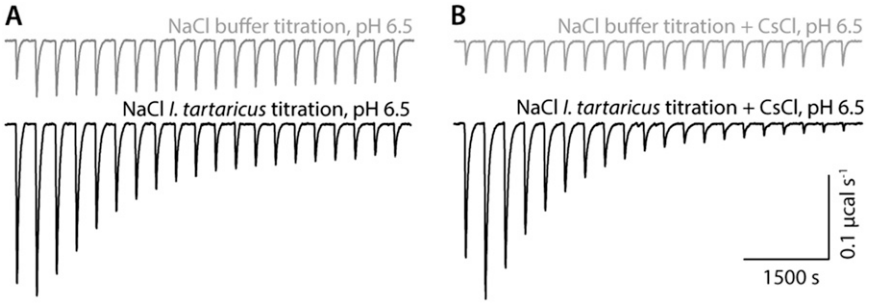

Fig. S1. Evidence of Na^+ binding to the *I. tartaricus* c-ring from ITC experiments. (*A*) Exothermic ITC signals measured in a representative NaCl titration of a protein sample [in 1% *n*-octyl-β-D-glucopyranoside (OG), 10 mM Mes/TMAOH buffer at pH 6.5] (black), compared with an equivalent titration of the buffer solution without the protein (gray); the magnitude of the signals before saturation reflect Na^+ binding to the protein, whereas those after saturation reflect the heat of dilution of the injected NaCl aliquots. (*B*) Comparison of ITC signals measured as in *A*, using a buffer containing CsCl (∼3 mM). Because Cs^+ does not bind to the c-ring (Fig. S2), CsCl can be used to preset the ionic strength of the buffer and thus minimize the heat of dilution of the injected NaCl aliquots.

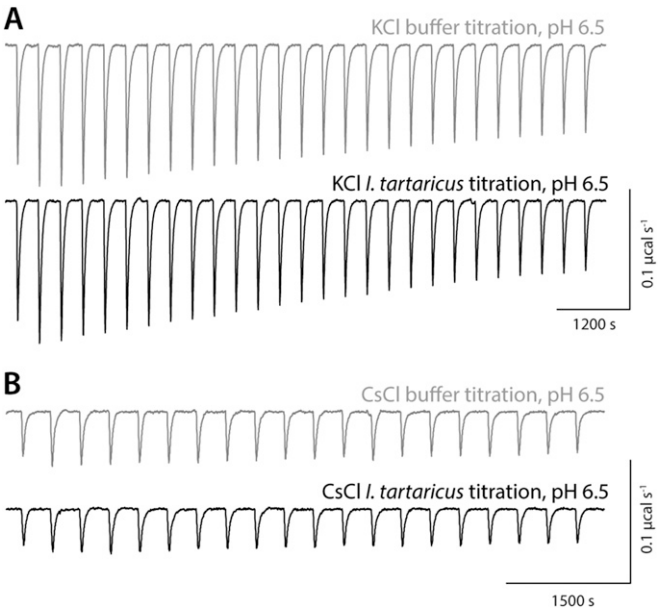

Fig. S2. Neither K^+ nor Cs^+ bind to the *I. tartaricus* c-ring. ITC signals measured in representative (*A*) KCl and (*B*) CsCl titrations of a protein sample (in 1% OG, 10 mM Mes/TMAOH buffer at pH 6.5) and of the buffer without protein. In both cases, the signals recorded for the c-ring samples are highly similar to those measured in the absence of the protein and thus reflect the heat of dilution of the injected KCl/CsCl aliquots, and not binding to the protein.

Fig. S3. The *I. tartaricus* c-ring is stable over a wide pH range and micromolar Na^+ concentrations. Purified c-ring samples were incubated overnight in 1% OG, 10 mM Mes/TMAOH at different pH values and at room temperature (i.e., the same buffer used in the ITC experiments). The Na^+ concentration of the samples was less than 10 µM, as measured by atomic absorption spectroscopy. A subsequent SDS/PAGE analysis of the samples demonstrates that the c_{11} complex is stable over the pH range considered, revealing no indication of dissociated c-subunit monomers.

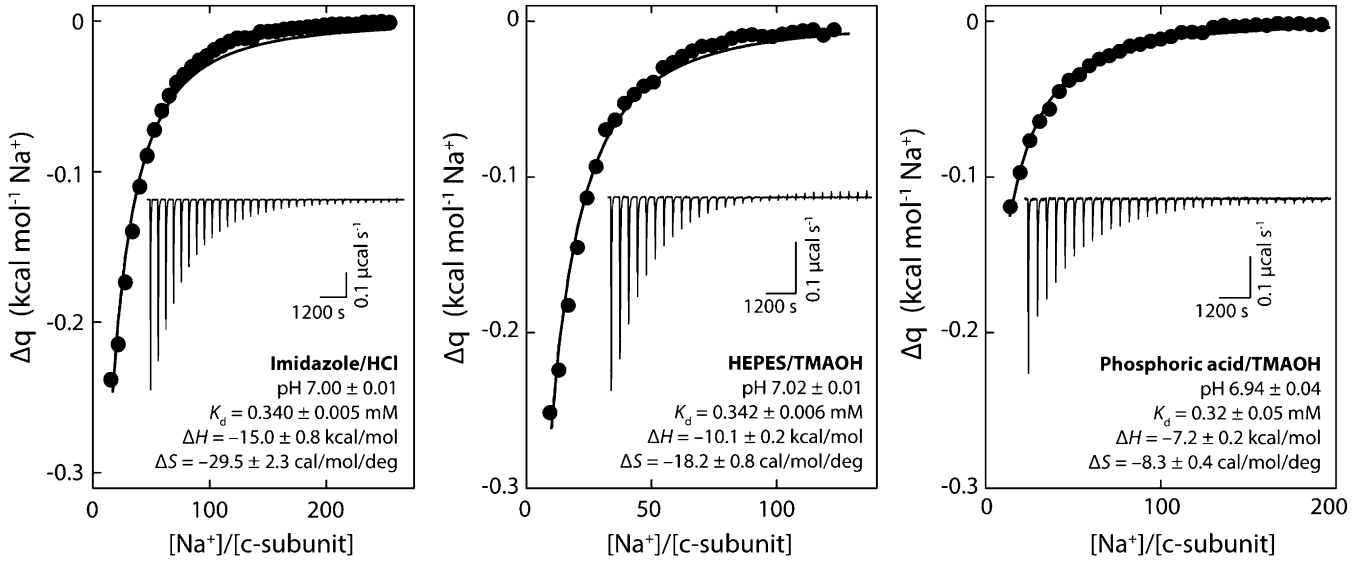

Fig. S4. Dependence between the apparent enthalpy of Na^+ binding and the enthalpy of ionization of the buffer. The figure shows ITC signals from representative NaCl titrations of c-ring samples in three different buffers (10 mM buffer, 1% OG, total ionic strength set to 60 mM) at pH 7 (*Insets*), alongside the corresponding binding isotherms (black circles, black curve) and thermodynamic parameters (obtained from two independent measurements for each buffer). Because the *I. tartaricus* c-ring does not have any histidine residues, the apparent enthalpy of Na^+ binding to the c-ring, ΔH, which also reflects H^+ release, should depend on the ionization enthalpy of the buffer, whereas the dissociation constant should not. The buffers used were imidazole/HCl, Hepes/TMAOH, and phosphoric acid/TMAOH. The published ionization enthalpy values for these buffers are 8.74 ± 0.01, 5.02 ± 0.02, and 1.22 ± 0.01 kcal/mol, respectively (1). Note that the ionization enthalpy of these buffers is largely independent of the ionic strength (2).

1. Fukada H, Takahashi K (1998) Enthalpy and heat capacity changes for the proton dissociation of various buffer components in 0.1 M potassium chloride. *Proteins* 33(2):159–166.
2. Goldberg RN, Kishore N, Lennen RM (2002) Thermodynamic quantities for the ionization reactions of buffers. *J Phys Chem Ref Data* 31(2):231–370.

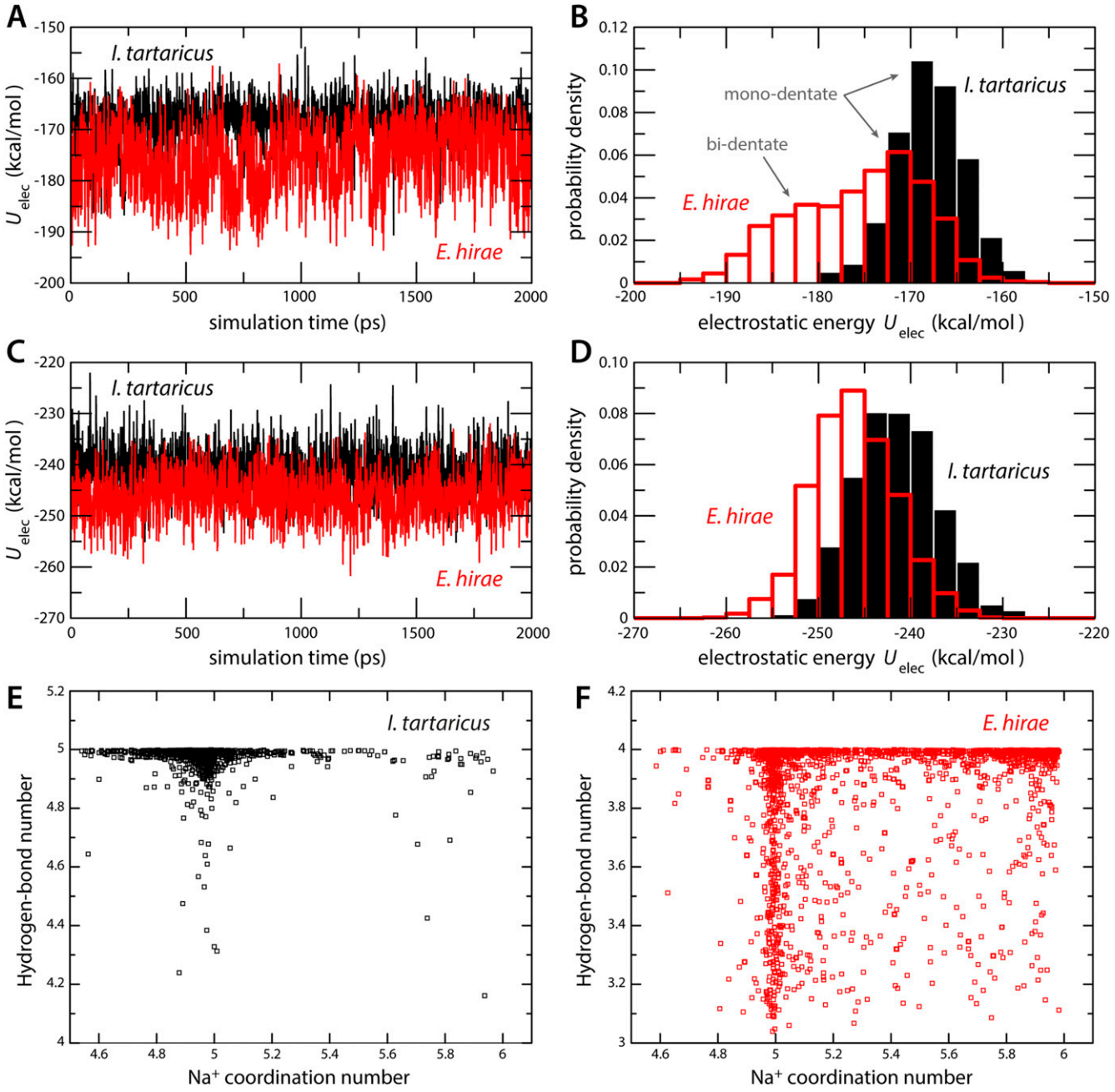

Fig. S5. Alternative modes of Na^+ coordination in the *I. tartaricus* and *E. hirae* c-rings. The figure analyzes the energetics and geometry of the Na^+-bound state for one of the binding sites in each c-ring, in 2,000 simulation snapshots over a 2-ns molecular dynamics trajectory. (*A* and *B*) Time series of the electrostatic interaction energy for the carboxyl-Na^+ pair in the *I. tartaricus* (black) and *E. hirae* (red) binding sites, alongside the probability distribution thereof. It is apparent that the *E. hirae* distribution is bimodal and that the mode not present in *I. tartaricus* (bidentate) results in a more favorable electrostatic energy. (*C* and *D*) Time series of the total ion–protein and protein–protein electrostatic interaction energy for Na^+ and all its coordinating groups, alongside the probability distribution thereof. The overall electrostatic energy of the Na^+-bound state remains more negative for the *E. hirae* c-ring. (*E* and *F*) The Na^+ coordination number is plotted against the number of hydrogen bonds between the protein residues (and water molecule) that form the Na^+-binding site (Fig. 5). A Na^+-coordination number of 5 corresponds to a monodentate interaction between Na^+ and the conserved glutamate in the binding site (E65 and E139, respectively); by contrast, a coordination number of 6 reflects a bidentate interaction (Fig. 5). The data shows that the bidentate mode is feasible in *E. hirae* but not in *I. tartaricus*. Moreover, it shows that the bidentate mode in *E. hirae* does not imply a loss of H-bonding interactions within the binding site, which indicates that this mode contributes significantly to the energetics of Na^+ binding, despite the fact that the monodentate mode is more probable (consistent with the X-ray structure of this c-ring); indeed, the H-bonding number for the bidentate mode is, on average, closer to the maximum value of 4. The Na^+-coordination number was determined as described in Fig. 5. The hydrogen bond number was defined as $N_{HB} = \Sigma_{ij}\,[1 - (r_{ij}/r_0)^{30}]\,[1 - (r_{ij}/r_0)^{60}]^{-1}$, where r_{ij} denotes the distances between pairs of atoms potentially engaged in hydrogen-bonding interactions within the ion-binding sites (in the Na^+-bound state), and $r_0 = 3.4$ Å. For *I. tartaricus*, five distance pairs were considered, namely E65:$O_{\varepsilon 1/2}$ – S66:O_γ, E65:$O_{\varepsilon 1/2}$ – Y70:O_H, E65:$O_{\varepsilon 1/2}$ – Q32:$N_{\varepsilon 2}$, T67:O_γ – G25:O, and W:O – T67:O_γ. In *E. hirae*, the maximum number of H-bonds is four, namely E139:$O_{\varepsilon 1/2}$ – T64:O_γ, E139:$O_{\varepsilon 1/2}$ – Y68:O_H, E139:$O_{\varepsilon 1/2}$ – Q110:$N_{\varepsilon 2}$, and Q65:$N_{\varepsilon 2}$ – Q110:$O_{\varepsilon 1}$.

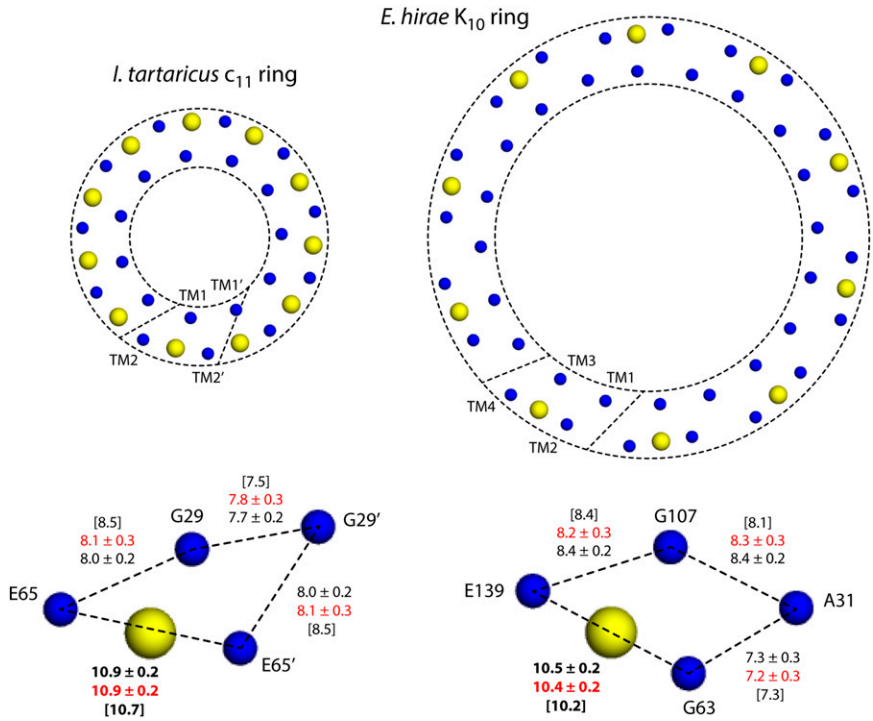

Fig. S6. Overall geometrical features of the *I. tartaricus* and *E. hirae* c-rings. The figure shows the location of representative Cα atoms in the inner and outer helices of each of the c- and K-subunits in each ring (blue spheres), alongside the bound Na^+ ions. Analysis of the distances between these Cα atoms demonstrates that the outer helices that flank the ion-binding sites in *E. hirae* are closer together than in *I. tartaricus*. This is likely due to the fact that the curvature of the outer ring of helices in *E. hirae* is much smaller than in *I. tartaricus*, owing to the greater size of the *E. hirae* ring (10 K-subunits of four helices each versus 11 c-subunits of two helices each) and to the greater separation between the inner helices.

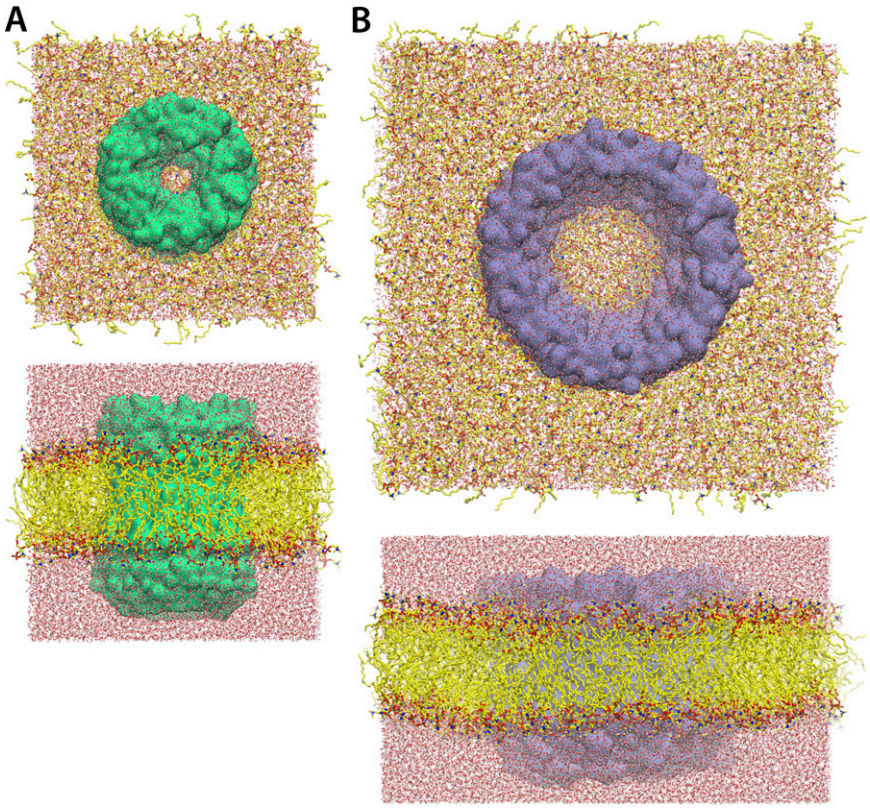

Fig. S7. All-atom molecular simulation models of the *I. tartaricus* and *E. hirae* c-rings. (*A*) The *I. tartaricus* c_{11}-ring, viewed from the cytoplasm (*Top*) and along the membrane plane (*Lower*). The simulation system includes 237 1-palmitoyl-2-oleoyl-*sn*-glycero-3-phosphocholine (POPC) (yellow carbon atoms) lipid molecules, ∼18,000 solvent water molecules (red oxygen atoms), summing up to a total of ∼100,000 atoms. (*B*) The *E. hirae* K_{10}-ring, viewed from the cytoplasm (*Top*) and along the membrane plane (*Lower*). The simulation system comprises 540 POPC molecules, ∼380,500 water molecules, and 10 Cl^- ions (added to counter the net charge of the ring), adding up to a total of ∼210,000 atoms. The central opening in the *I. tartaricus* ring is occluded by two POPC molecules on the cytoplasmic side and three molecules on the periplasmic side. In the *E. hirae* ring, the much wider central opening allows for 18 and 17 POPC molecules on the cytoplasmic and periplasmic sides, respectively.

Table S1. Ion coordination distances in the most probable configurations of the Na^+- and H^+-bound states in simulations of the *I. tartaricus* and *E. hirae* c-rings

c-Ring	Interaction	Distance, Å
I. tartaricus		
Na^+-bound state (monodentate configuration)	Na^+ – E65:Oε_2	2.16 ± 0.07
	Na^+ – S66:Oγ	2.3 ± 0.1
	Na^+ – V63:O	2.3 ± 0.1
	Na^+ – Q32:Oε_1	2.3 ± 0.1
	Na^+ – W:O	2.3 ± 0.1
H^+-bound state (most populated cluster)	E65:Oε_1 – Y70:O_H	2.9 ± 0.2
	E65:Oε_2 – S66:Oγ	2.8 ± 0.1
E. hirae		
Na^+-bound state (monodentate configuration)	Na^+ – E139:Oε_2	2.15 ± 0.07
	Na^+ – T64:Oγ	2.3 ± 0.1
	Na^+ – L61:O	2.3 ± 0.1
	Na^+ – Q110:Oε_1	2.3 ± 0.1
	Na^+ – Q65:Oε_1	2.3 ± 0.1
H^+-bound state (most populated cluster)	E139:Oε_1 – Y68:O_H	2.8 ± 0.2
	E139:Oε_2 – T64:Oγ	2.8 ± 0.1